

## RESEARCH ARTICLE

# Peptide-based systems analysis of inflammation induced myeloid-derived suppressor cells reveals diverse signaling pathways

Waeowalee Choksawangkar<sup>1,2</sup>, Lauren M. Graham<sup>1</sup>, Meghan Burke<sup>1</sup>, Sang Bok Lee<sup>1,3</sup>, Suzanne Ostrand-Rosenberg<sup>4</sup>, Catherine Fenselau<sup>1</sup> and Nathan J. Edwards<sup>5</sup>

<sup>1</sup> Department of Chemistry and Biochemistry, University of Maryland, College Park, MD, USA

<sup>2</sup> Department of Biochemistry, Faculty of Science, Burapha University, Chonburi, Thailand

<sup>3</sup> Graduate School of Nanoscience and Technology (WCU), Korea Advanced Institute of Science and Technology, Daejeon, Korea

<sup>4</sup> Department of Biological Sciences, University of Maryland Baltimore County, Baltimore, MD, USA

<sup>5</sup> Department of Biochemistry and Molecular & Cellular Biology, Georgetown University Medical Center, Washington, DC, USA

A better understanding of molecular signaling between myeloid-derived suppressor cells (MDSC), tumor cells, T-cells, and inflammatory mediators is expected to contribute to more effective cancer immunotherapies. We focus on plasma membrane associated proteins, which are critical in signaling and intercellular communication, and investigate changes in their abundance in MDSC of tumor-bearing mice subject to heightened versus basal inflammatory conditions. Using spectral counting, we observed statistically significant differential abundances for 35 proteins associated with the plasma membrane, most notably the pro-inflammatory proteins S100A8 and S100A9 which induce MDSC and promote their migration. We also tested whether the peptides associated with canonical pathways showed a statistically significant increase or decrease subject to heightened versus basal inflammatory conditions. Collectively, these studies used bottom-up proteomic analysis to identify plasma membrane associated pro-inflammatory molecules and pathways that drive MDSC accumulation, migration, and suppressive potency.

Received: March 17, 2015

Revised: May 3, 2016

Accepted: May 16, 2016

## Keywords:

Cell migration / Differential protein expression / Immune suppression / Inflammation / Mass spectrometry – LC-MS/MS / Myeloid-derived suppressor cells / Systems biology



Additional supporting information may be found in the online version of this article at the publisher's web-site

## 1 Introduction

Chronic inflammation is associated with tumor promotion and progression [1, 2]. Previous studies have demonstrated that a group of immune suppressive cells, referred to as

myeloid-derived suppressor cells (MDSC), are induced by inflammation and strongly facilitate tumor growth and metastasis. MDSC are immature myeloid cells that exhibit potent suppressive activities for both innate and adaptive immunity [3]. In normal conditions, myeloid progenitor cells differentiate in the bone marrow, and the mature cells migrate to peripheral organs. However, in cancer, the immature MDSC traffic to the blood and peripheral organs and ultimately migrate into tumor sites [4]. Inflammatory mediators secreted by malignant cells and host cells are potent inducers of MDSC and heighten their immune suppressive activities [1, 5–9].

It has been recognized that the inflammation-driven migration and accumulation of MDSC play important roles in

**Correspondence:** Dr. Nathan J. Edwards, Department of Biochemistry and Molecular & Cellular Biology, Georgetown University Medical Center, Washington, DC 20057, USA

**E-mail:** nje5@georgetown.edu

**Abbreviations:** IL-1 $\beta$ , interleukin-1 beta; MDSC, myeloid-derived suppressor cells; PM, plasma membrane; PMCBA, plasma membrane coating buffer A; PSM, peptide-spectrum-matches; SAGE, serial analysis of gene expression

## Significance of the study

This study applies a bottom-up proteomics analysis of plasma membrane associated proteins derived from mouse tumor-induced myeloid-derived suppressor cells (MDSC) generated under heightened inflammatory conditions. Inflammatory mediators secreted by malignant cells and host cells induce MDSC and heighten their suppressive potency of innate and adaptive immunity. The workflow uses a previously described pellicle method to enrich plasma membrane associated proteins from the MDSC, and compares protein abundance in basal vs. heightened inflammatory conditions using spectral counting. Statistical significance of differ-

entially abundant proteins is assessed using Fisher's exact test. Pro-inflammatory and chemotactic proteins S100A8 and S100A9 are observed to be associated with the MDSC plasma membrane, where they are readily available for intercellular signaling, and demonstrate significantly increased abundance under inflammatory conditions. A novel pathway analysis strategy, also using Fisher's exact test, was used to identify significantly perturbed canonical pathways including a number related to integrin signaling, elucidating functional elements of the complex process of immunosuppression.

the failure of cancer immunotherapy and that depletion of MDSC enhances the function of antitumor T-cell activities. A better understanding of molecular signaling between MDSC, tumor cells, T-cells, and inflammatory mediators is expected to contribute to the development of more effective cancer immunotherapies. Plasma membrane (PM) proteins of MDSC are potential targets for signaling mechanisms that activate these cells, and in this study we focus on the changes in the MDSC plasma membrane associated proteome when the level of inflammation is increased, as is commonly the case in some tumor microenvironments. We have employed MS-based semi-quantitative proteomic analysis to investigate the abundance differences between the PM associated proteins of MDSC induced in basal inflammatory and heightened inflammatory environments. The MDSC induced under lower levels of inflammation are designated "conventional MDSC;" while those induced under heightened levels of inflammation are denoted "inflammatory MDSC." Both MDSC populations are obtained from BALB/c mice carrying 4T1 mammary carcinoma tumors and characterized by flow cytometry. Heightened inflammatory conditions were generated using 4T1 cells transfected with and expressing high levels of the pro-inflammatory cytokine IL-1 $\beta$  [8].

In this study, we use a nanoparticle pellicle technique to enrich PM proteins prior to MS and filter identified proteins using plasma membrane related Gene Ontology annotations. This analysis strategy identifies, as plasma membrane proteins, both integral cell surface proteins spanning the lipid bilayer and peripheral proteins not traditionally thought of as part of the PM. The pellicle method has been described previously and evaluated using Western blots and spectral counting [10–16]. In each case, the technique resulted in the enrichment of PM proteins but identified both traditional PM proteins and proteins not traditionally considered part of the plasma membrane. We use a post-identification GO-based filter to further focus the analysis on PM and PM associated proteins, as some of the proteins identified after the pellicle enrichment are not known to be associated with the PM.

## 2 Materials and methods

Iron (III) chloride ( $\text{FeCl}_3 \cdot 6\text{H}_2\text{O}$ , 97.0%) was purchased from Alfa Aesar (Ward Hill, MA). Optima LC/MS grade acetonitrile, Poly(acrylic acid) (MW = 100 000) and protease inhibitor cocktail were purchased from Sigma-Aldrich (St. Louis, MO). Trypsin and endoproteinase Lys-C were supplied by Promega (Madison, WI). RCDCTM protein assay kit was purchased from Bio-Rad (Hercules, CA). TopTip C18 micro-spin columns were purchased from Glygen Corporation (Columbia, MD). Deionized water was produced using a Milli-Q A10 system (Millipore, Billerica, MA). BALB/c mice were obtained from Jackson Laboratory (Bar Harbor, ME). The 4T1 cell line derived from a BALB/c spontaneous mammary carcinoma [17] was kindly provided by Dr. Fred R. Miller from the Michigan Cancer Foundation.

### 2.1 Mice and cell lines

Wild type BALB/c mice were bred and maintained according to the NIH guidelines for the humane treatment of laboratory animals in the University of Maryland Baltimore County animal facility. All animal procedures were approved by the university's Institutional Animal Care and Use Committee. The 4T1 mammary carcinoma cell line and the transfected 4T1/IL1 $\beta$  cell line were maintained as previously described [8, 18].

### 2.2 MDSC harvesting and characterization

BALB/c mice were inoculated in the abdominal mammary gland with 4T1 or 4T1/IL1 $\beta$  tumor cells, and MDSC were harvested from the mice as described by Chornoguz et al. [9]. Briefly, mice with primary 4T1 or 4T1/IL1 $\beta$  tumors of ~7–10 mm in diameter and established metastatic disease were bled from the submandibular vein into heparinized tubes. Red blood cells were removed by lysis and the remaining

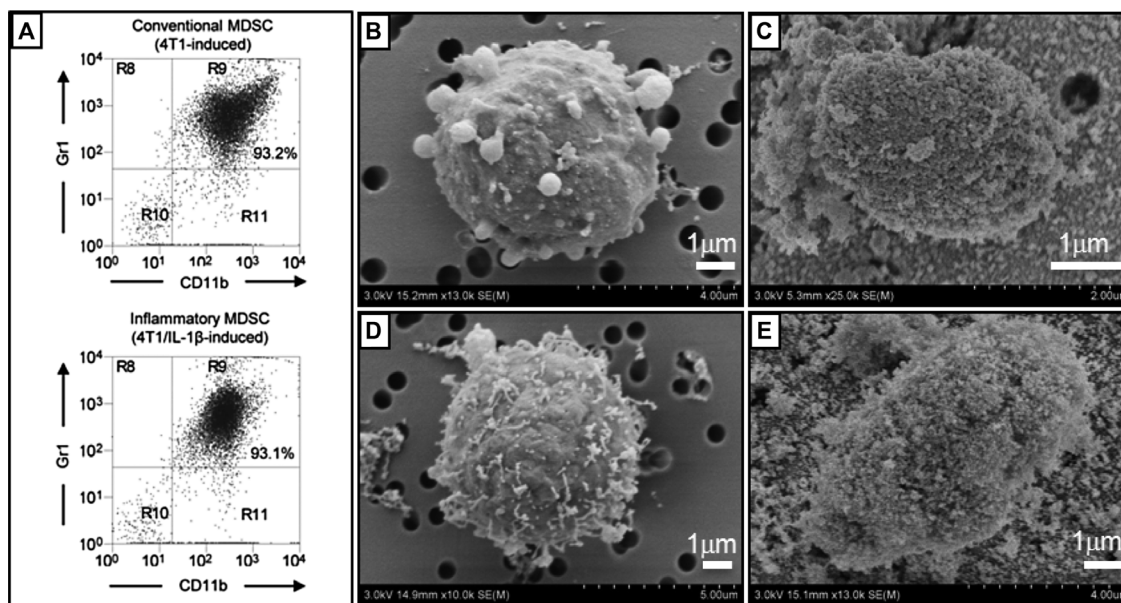


**Figure 1.** (A) Representative flow cytometry analysis of conventional and inflammatory MDSC isolated from BALB/c mice with large 4T1 or 4T1/IL-1 $\beta$  mammary carcinoma tumors, labeled by immunofluorescence for the MDSC plasma membrane markers Gr1 and CD11b. (B) – (E) Morphology of the cells: (B) conventional MDSC, (C) Fe<sub>3</sub>O<sub>4</sub> nanoparticle-coated conventional MDSC, (D) inflammatory MDSC, and (E) Fe<sub>3</sub>O<sub>4</sub> nanoparticle-coated inflammatory MDSC.

leukocytes were used immediately or frozen at  $-80^{\circ}\text{C}$  until used. The percent of MDSC in the ex vivo leukocyte population was determined by immunofluorescence and flow cytometry using the fluorescent antibodies Gr1-FITC and CD11b-PE (eBioscience, Inc., San Diego, CA) as described [9]. Individual biological samples consisted of MDSC pooled from two to three individual mice and consisted of  $>90\%$  Gr1<sup>+</sup> CD11b<sup>+</sup> cells (see Fig. 1A).

### 2.3 Synthesis of Fe<sub>3</sub>O<sub>4</sub> nanoparticles

Fe<sub>3</sub>O<sub>4</sub> nanoparticles were synthesized using the polyol method previously described by Ammar et al. [19,20]. Briefly, 1,2-propanediol solution containing 8 mM iron (III) chloride, 24 mM sodium acetate, and 2 mL water was refluxed for 15 h. The nanoparticles were extracted from solution with a neodymium magnet, washed with water and dispersed for 24 h in a solution of 20 mM Al(NO<sub>3</sub>)<sub>3</sub> and 100 mM KNO<sub>3</sub>, adjusted to pH 7. The Al<sub>2</sub>O<sub>3</sub> coated Fe<sub>3</sub>O<sub>4</sub> nanoparticles were rinsed and briefly stored in PBMCA buffer (pH 7.4) until cell coating experiments were performed. Characterization of the particles was achieved with a JEOL JEM-2100F Field Emission TEM (JEOL USA, Inc., Peabody, MA) with scanning TEM and Oxford energy dispersive x-ray spectrometry capabilities, and a Zetasizer Nano ZS90 particle analyzer (Malvern Instruments Ltd, Worcestershire WR14 1XZ, UK). Analysis of the particle size showed an average diameter of  $17 \pm 6$  nm. The surface charge was determined as a positive potential of  $64 \pm 3$  mV. To further confirm the presence of the Al<sub>2</sub>O<sub>3</sub> functional group, an elemental analysis was performed

using an EDX measurement (Supporting Information Fig. 1).

### 2.4 Pellicle construction and cell lysis

The pellicle was constructed following our previously published procedure with minor modifications [10, 11]. Preparation of the plasma membrane pellicles on conventional and inflammatory MDSC was performed in parallel. Approximately  $1 \times 10^8$  MDSC from each type were resuspended in 2 mL PMCBA (800 mM sorbitol, 20 mM MES, 150 mM NaCl, pH 5.3) and added dropwise to a 10% (w/v) Al<sub>2</sub>O<sub>3</sub> coated Fe<sub>3</sub>O<sub>4</sub> suspension. Coating was performed at  $4^{\circ}\text{C}$  by gently rocking the mixture for 15 min. Excess nanoparticles were removed by collecting the nanoparticle-coated cells at  $900 \times g$  for 5 min and washing three times. The coated cells were cross-linked by adding the suspension to 10 mg/mL poly(acrylic acid) in PMCBA, pH 6.0–6.5, in a dropwise fashion, and incubated at  $4^{\circ}\text{C}$  for 15 min with gentle rocking. The cross-linked cells were collected by centrifugation at  $900 \times g$  for 5 min and washed with PMCBA to remove excess poly(acrylic acid). The cell pellet was placed in 2.5 mM imidazole with protease inhibitor cocktail and incubated on ice for 30 min to swell the cells. Cell lysis was carried out by using N<sub>2</sub> cavitation at 1500 psi for 30 min. The cell lysate was spun at  $100 \times g$  for 7 min to isolate the PM nanoparticle pellicles from cellular organelles and lysates, and washed three times with the lysis buffer, three times with 1 M Na<sub>2</sub>CO<sub>3</sub>, pH 11.4, and another three times with 1 M KCl. Proteins were released from the pellicles by triplicate extractions in 2% SDS, 62.5 mM

Tris-HCl, and 5%  $\beta$ -mercaptoethanol, at 100°C for 5 min in a lab microwave oven (CEM Corporation, Matthews, NC). The protein concentration was measured using an RCDC™ protein assay kit, prior to 1D-gel electrophoresis or proteolysis in-solution.

## 2.5 Scanning electron microscopy

Cells were prepared for imaging by a Hitachi SU-70 Field Emission scanning electron microscope and a Hitachi S-4700 Field Emission scanning electron microscope (Hitachi, Gaithersburg, MD) as previously reported [10].

## 2.6 Proteomic analysis by HPLC-MS/MS

One hundred micrograms of protein recovered from the pellicle in 2% SDS was precipitated using chloroform/methanol [21], and resolubilized in 8 M urea in 50 mM  $\text{NH}_4\text{HCO}_3$ . The proteins were reduced and alkylated by iodoacetamide. Lys-C digestion was carried out in 8 M urea/50 mM  $\text{NH}_4\text{HCO}_3$  solution at 37°C for 3 h, using an enzyme to protein ratio of 1:50. After five-fold dilution, tryptic digestion was performed at 37°C for 16 h, using an enzyme to protein ratio of 1:25. The digests were desalted for LC-MS/MS analysis.

LC-MS/MS analysis was performed using a Shimadzu Prominence nanoHPLC (Shimadzu, Columbia, MD) interfaced to an LTQ-orbitrap XL (ThermoFisher Scientific, San Jose, CA). Peptides from 15  $\mu\text{g}$  proteins were fractionated in a Vydac Everest C18 column (150 mm x 150  $\mu\text{m}$ ) with 300 Å pore size and 5  $\mu\text{m}$  particle size (Grace Vydac, Deerfield, IL), using a flow rate of 500 nL/min. A linear gradient was increased from 0 to 60% solvent B (97.5% acetonitrile, 2.5%  $\text{H}_2\text{O}$ , 0.1% formic acid) in 90 min, and then from 60 to 85% solvent B for 20 min. The samples were ionized using a spray voltage of +1.8 kV, a tube lens voltage of 100 kV, and a capillary temperature of 275°C. The mass spectrometer was operated in a data-dependent mode. Precursor ions were scanned in the orbitrap at a resolution set for 30 000 at  $m/z$  400. In each cycle, the nine most abundant ions above the threshold of 50 000 ions were isolated for collision-induced dissociation (CID), using a normalized collision energy of 35 and an activation time of 30 ms, followed by product ion scans in the LTQ. The precursor ions were isolated using an isolation window of 3 Da. Dynamic exclusion was enabled with a repeat count of 1 and duration of 180 s. For label-free quantitation, two to six replicate injections were performed to maximize the identification of low abundance proteins, in the three biological replicates.

## 2.7 Bioinformatics

Spectra in RAW format were subjected to centroiding and mzXML reformatting using msconvert [22]. All data sets

were searched against UniProt mouse reference proteome using PepArML [23, 24]. Carbamidomethylation of cysteine was specified as a fixed modification, and oxidation of methionine residues specified as a variable modification. Search results were filtered at 1% spectral FDR. A global protein parsimony analysis was used to infer proteins, subject to at least two unshared peptides per protein, resulting in 428 inferred proteins with estimated protein FDR of 0.46% (Supporting Information Tables 1 and 2).

Subcellular localization of proteins was determined using UniProt Gene Ontology annotations [25] and an in-house GO Slim of specific GO cellular compartment terms, including “plasma membrane.” Cellular proteins are highly dynamic and are present in multiple organelles [26] – this is reflected in the GO cellular compartment annotations [27], curated from published manuscripts, which may result in proteins not traditionally considered membrane proteins receiving a “plasma membrane” annotation. In this study, proteins annotated via the GO Slim with “plasma membrane” were considered to be plasma membrane associated proteins and retained for differential protein and pathway analysis.

To compare protein abundance between treatments, in-house software was developed to determine the spectral count, after spectral FDR-based filtering and protein parsimony analysis, of inferred proteins. Under the null-hypothesis that proteins in the two treatment conditions are not differentially abundant, we expect the spectral counts for a specific protein to reflect the total number of PSMs observed in each condition. Fisher’s exact test was used to calculate the statistical significance of the imbalance in the spectral counts for each protein [28]. To correct for multiple testing, the FDR was determined using the Benjamini-Hochberg method [29]. The ratio of spectral counts ( $R_{SC}$ ), which provides an estimate of the fold-change between two samples, was computed using the serial analysis of gene expression (SAGE) [30] procedure, as described by Old et al. [31].

Pathway analysis was carried out using canonical pathway gene-sets from Molecular Signatures Databases (MSigDB) 4.0 [32] collection C2, which includes KEGG, REACTOME, and PID pathway databases. Since MSigDB provides gene-sets only for human genes, identified proteins’ UniProt accessions were first mapped to mouse genes and then to orthologous human genes, using the UniProt gene names and NCBI’s HomoloGene. Traditional pathway enrichment analysis of differentially abundant human genes was carried out using candidate gene-lists constructed using Fisher’s exact test FDR < 10% and increased, decreased, or increased and decreased spectral counts in inflammatory MDSC. The set of all identified genes was used as the pathway enrichment background. Fisher’s exact test, and Benjamini-Hochberg FDR, was used to assess the statistical significance of the number of genes in common between each canonical pathway and the various candidate gene-lists.

A novel peptide-based pathway analysis was also applied to canonical pathway gene-sets from MSigDB 4.0. Identified

**Table 1.** Plasma membrane associated proteins with significant increase of abundance in response to inflammation ( $|R_{SC}| \geq 1$  and Fisher's exact test FDR  $\leq 5\%$ )

Accession	Gene	Description	$ R_{SC} $	FDR
P27005	S100a8	Protein S100-A8	1.75	8.04E-33
P31725	S100a9	Protein S100-A9	1.24	5.78E-21
Q00612	G6pdx	Glucose-6-phosphate 1-dehydrogenase X	2.02	1.63E-12
P11276	Fn1	Fibronectin	4.99	6.77E-12
Q61233	Lcp1	Plastin-2	1.75	7.06E-12
P52480	Pkm	Pyruvate kinase PKM	1.29	7.72E-11
Q8VCM7	Fgg	Fibrinogen gamma chain	4.12	1.54E-10
Q8K0E8	Fgb	Fibrinogen beta chain	4.78	2.17E-10
P40124	Cap1	Adenylyl cyclase-associated protein 1	1.36	4.24E-08
P20152	Vim	Vimentin	2.62	5.03E-05
P26041	Msn	Moesin	1.45	7.09E-05
Q61096	Prtn3	Myeloblastin	1.51	1.10E-04
Q9WVK4	Ehd1	EH domain-containing protein 1	3.46	5.94E-04
P04919	Slc4a1	Band 3 anion transport protein	1.37	8.69E-04
Q61210	Arhgef1	Rho guanine nucleotide exchange factor 1	2.51	9.71E-04
Q8CIZ8	Vwf	von Willebrand factor	3.23	2.39E-03
Q9CVB6	Arcp2	Actin-related protein 2/3 complex subunit 2	2.34	3.35E-03
P11499	Hsp90ab1	Heat shock protein HSP 90-beta	1.00	9.37E-03
Q63844	Mapk3	Mitogen-activated protein kinase 3	2.95	9.85E-03
P26040	Ezr	Ezrin	1.07	2.57E-02
O08808	Diaph1	Protein diaphanous homolog 1	1.15	2.87E-02
Q9QUM0	Itga2b	Integrin alpha-IIb	2.20	3.46E-02

proteins were associated with human genes, as previously described. The number of distinct peptides associated with each gene-set's genes were determined for conventional and inflammatory MDSC. To assess the statistical significance of the change in distinct peptide count for each treatment, Fisher's exact test was applied to each pathway's distinct peptide counts with respect to all distinct peptides, and Benjamini-Hochberg FDR computed to correct for multiple testing.

### 3 Results and discussion

Circulating MDSC were harvested from mice with 4T1 or 4T1/IL-1 $\beta$  tumors and stained with fluorescently coupled antibodies to the markers characteristic of MDSC (Gr1 and CD11b). Figure 1 indicates that around 93% of the cells used in the experiment are Gr1<sup>+</sup>CD11b<sup>+</sup>. Plasma membrane associated proteins from these highly purified MDSC were enriched by the pellicle technique using Al<sub>2</sub>O<sub>3</sub>-coated Fe<sub>3</sub>O<sub>4</sub> nanoparticles. Cell surface morphology of MDSC observed by SEM is shown in Fig. 1B and D. Both conventional and inflammatory MDSC exhibited extrusions of various sizes and microvilli. Observations of multiple cells indicate that there is no substantial change in morphology between the two types of MDSC. Most of the MDSC are approximately 5  $\mu$ m in diameter, smaller than many other types of cells. Micrographs in Fig. 1C and E indicate successful coating of the nanoparticles on the MDSC surfaces.

Protein analysis identified 140 PM associated proteins satisfying the two unshared peptide constraint in conventional

MDSC and 164 PM associated proteins in inflammatory MDSC; of these 117 proteins are in common. In the combined dataset of plasma membrane annotated proteins, 191 proteins satisfy the two unshared peptide constraint (Supporting Information Tables 3 and 4). In the enriched samples about 45% of the identified UniProt proteins are annotated with the GO Slim term "plasma membrane." Semi-quantitative analysis using spectral counting was performed on the pooled peptide identifications of conventional and inflammatory MDSC. Changes in protein abundance were calculated and normalized using serial analysis of gene expression, which provides a correction factor for the fold change to avoid discontinuity of the data in case that a given protein is identified in only one sample, and statistical significance assessed by Fisher's exact test and Benjamini-Hochberg FDR (Supporting Information Table 5). Relative protein abundance expressed as log<sub>2</sub> ratios between inflammatory and conventional MDSC ( $R_{SC}$ ) of absolute value greater than 1 and FDR less than 5% were considered to be significantly changed. From the total of 191 PM associated proteins identified, 22 proteins were shown to have significantly higher abundance in inflammatory MDSC (Table 1), and 13 proteins were observed to have significantly lower abundance (Table 2). Proteins S100A8 and S100A9 show the most significant increase. Previous studies suggest that S100A8 and S100A9 form a heterodimer in exosomes released by MDSC facilitate the migration of MDSC into the tumor microenvironment via an NF- $\kappa$ B-dependent pathway [7, 34]. S100A8 and S100A9 also drive the accumulation of MDSC by inhibiting normal myelopoiesis via a STAT3-dependent pathway [33]. The increased abundances observed here are in agreement with a previous report in

**Table 2.** Plasma membrane associated proteins with significant decrease of abundance in response to inflammation ( $|R_{sc}| \geq 1$  and Fisher's exact test FDR  $\leq 5\%$ )

Accession	Gene	Description	$ R_{sc} $	FDR
P28293	Ctsg	Cathepsin G	1.78	6.83E-13
Q8VDN2	Atp1a1	Sodium/potassium-transporting ATPase subunit alpha-1	2.67	4.13E-09
P08752	Gnai2	Guanine nucleotide-binding protein G(i) subunit alpha-2	1.03	3.11E-07
Q9QXS1	Plec	Plectin	2.67	4.46E-06
P51437	Camp	Cathelin-related antimicrobial peptide	1.30	3.91E-05
Q5SUA5	Myo1g	Unconventional myosin-Ig	1.45	1.37E-04
P24063	Itgal	Integrin alpha-L	1.75	1.39E-04
Q61735	Cd47	Leukocyte surface antigen CD47	1.28	1.71E-03
P57787	Slc16a3	Monocarboxylate transporter 4	1.28	2.26E-03
Q62178	Sema4a	Semaphorin-4A	2.48	1.46E-02
P04104	Krt1	Keratin, type II cytoskeletal 1	1.03	1.52E-02
Q61462	Cyba	Cytochrome b-245 light chain	1.81	1.98E-02
Q9JIZ9	Plscr3	Phospholipid scramblase 3	1.85	2.98E-02

which western blotting demonstrated increases in the level of S100A8/S100A9 in the inflammatory environment [7].

Pathway enrichment analysis was carried out using differentially abundant PM associated proteins and the canonical pathways of the MSigDB C2 collection. After mapping UniProt mouse protein accessions to human genes, a total of 183 genes were considered identified and used as the background gene-list, with 31 genes increased and 32 decreased in inflammatory MDSC. A total of 1320 canonical pathways from KEGG, REACTOME, and PID were evaluated for a statistically surprising high (or low) number of genes intersecting with increased, decreased, or increased and decreased candidate gene lists using Fisher's exact test at 10% FDR (Supporting Information Table 6). Unfortunately, given the small magnitude of the candidate and background gene-lists, no pathways were found to have a statistically significant number of intersecting genes after multiple test correction. A similar analysis was carried out on the UniProt mouse protein accessions using the DAVID Bioinformatics tool, with a similar lack of statistically significant pathways observed (data not shown).

A novel peptide-based pathway analysis strategy was implemented for a more sensitive detection of perturbed pathways than the traditional approach. Mouse peptides originally identified from mouse protein sequences were associated with MSigDB 4.0 C2 collection canonical pathways via mouse, then human genes. Distinct peptides, tabulated for each pathway gene-set for conventional vs inflammatory MDSC, can be formed into a contingency matrix for Fisher's exact test. The test determines whether a gene set's distinct peptide count specific to inflammatory or conventional MDSC is surprisingly high or low. If the genes of a gene-set are not differentially abundant, the number of treatment specific gene-set distinct peptides should be consistent with the total number of conventional or inflammatory specific distinct peptides. We evaluate treatment specific peptides as some peptides are common to both treatments. Table 3 and Supporting Information Table 7 show the MSigDB canonical pathways with

at least four identified genes and Fisher's exact test FDR less than 1% for differential peptide counts. This approach identifies 13 canonical pathways with more distinct peptides than expected in inflammatory MDSC, and three canonical pathways with less distinct peptides than expected in conventional MDSC.

We point out that the pathways found to be statistically significant in the peptide-based analysis were also evaluated by the traditional candidate gene-list based pathway enrichment analysis, but were not statistically significant. For example, the most significant of the gene-sets listed in Table 3 by the traditional approach is "REACTOME: Response to elevated platelet cytosolic Ca<sup>2+</sup>," which shares seven genes with the candidate gene-list defined by increased spectral counts (at FDR 10%) in inflammatory MDSC, resulting in (uncorrected) Fisher's exact test *p*-value 1.72E-3 and multiple-test corrected FDR of 0.57, which is not statistically significant. The most significant pathway of Table 3, "PID: Beta1 integrin cell surface interactions" has (uncorrected) *p*-value 0.016 using traditional pathway enrichment analysis, based on three genes in common with the same candidate gene-list of differentially abundant genes, also not significant once adjusted for multiple-testing. Importantly, in addition to the apparent improvement in sensitivity provided by the peptide-based approach, the peptide-based strategy does not require the somewhat arbitrary selection of thresholds for candidate gene-lists of differentially abundant genes (or proteins).

In the peptide-based analysis, the majority of the significant pathways involve members of the integrin family. Integrins, in general, are membrane glycoproteins known to regulate cellular migration and communication in the extracellular matrix [32]. Several proteins from the integrin family have been recognized in MDSC and proposed as cell surface markers for sub-populations, and one of the canonical markers of MDSC, CD11b, is an integrin [35, 36]. Although little is known about the functions of integrins in MDSC, published reports have revealed that other myeloid cells express integrins which facilitate their migration to the tumor

**Table 3.** Canonical pathways with significant increase or decrease of distinct peptides in response to inflammation. Pathways with an increase (decrease) in distinct peptides under inflammatory treatment shown above (below) the dotted line

Database: Description	Identified genes	Conventional peptides	Inflammatory peptides	FDR
PID: Beta1 integrin cell surface interactions	4	1	24	5.01E-09
PID: Beta3 integrin cell surface interactions	6	4	30	9.49E-09
KEGG: Pathways in cancer	12	22	62	1.79E-07
KEGG: ECM-receptor interaction	5	3	22	5.15E-06
REACTOME: Response to elevated platelet cytosolic Ca <sup>2+</sup>	13	60	111	3.15E-05
KEGG: Prostate cancer	5	10	31	2.94E-04
KEGG: NOD-like receptor signaling pathway	4	9	29	2.94E-04
PID: Integrins in angiogenesis	4	6	24	6.65E-04
BIOCARTA: How Progesterone Initiates Oocyte Membrane	4	7	25	1.18E-03
REACTOME: Platelet activation, signaling and aggregation	24	103	157	1.52E-03
REACTOME: Innate immune system	5	13	32	3.19E-03
PID: Syndecan-4-mediated signaling events	6	14	35	5.44E-03
KEGG: Pathogenic Escherichia coli infection	6	54	81	6.04E-03
<hr/>				
PID: Integrin family cell surface interactions	4	71	49	1.53E-04
PID: amb2 Integrin signaling	8	112	97	2.02E-05
KEGG: Cell adhesion molecules	4	84	53	1.24E-08

microenvironment [37, 38]. Since MDSC are present at high levels within solid tumors and must migrate to tumors from the bone marrow and blood, it is likely that integrins, such as those identified in this study, are involved in MDSC localization.

#### 4 Concluding remarks

We have integrated a plasma membrane enrichment technique with label-free semi-quantitative proteomic analysis to characterize changes in abundances of plasma membrane associated proteins when MDSC are stimulated by enhanced inflammation. This work confirms by direct measurement that the abundances of the chemotactic proteins S100A8 and S100A9 are increased in the presence of inflammation. We also show (Table 3) that inflammation is associated with increases in the abundances of proteins involved in several pathways that are classically associated with cell migration [35–38]. Our observations provide mechanistic support for the hypothesis that inflammation stimulates migration of MDSC into the tumor microenvironment.

We thank Dr. Yan Wang, Director of Proteomic Core Facility, Maryland Pathogen Research Institute, University of Maryland, College Park, for advice about the LC-MS/MS analysis, Dr. Sung-Young Kim for advice about the synthesis of the Fe<sub>3</sub>O<sub>4</sub> nanoparticles, and Ms. Virginia Clements for technical support in generating MDSC. We acknowledge Tim Maugel, Director of the Laboratory for Biological Ultrastructure, University of Maryland, College Park, for advice about SEM imaging. This research was supported by a grant from the National Institutes of Health, GM 021248. S.B.L. also thanks to the WCU program through the National Research Foundation of Korea funded by the Ministry of Education, Science and Technology, R31-2008-000-10071-0.

W.C. acknowledges a Royal Thai Government Fellowship. We acknowledge the support of the Maryland NanoCenter and its NispLab. The NispLab is supported in part by the National Science Foundation as an MRSEC Shared Experimental Facility.

The authors declare that they have no financial or commercial conflicts of interest.

#### 5 References

- [1] Ostrand-Rosenberg, S., Sinha, P., Myeloid-derived suppressor cells: linking inflammation and cancer. *J. Immunol.* 2009, *182*, 4499–4506.
- [2] Lu, H., Ouyang, W., Huang, C., Inflammation, a key event in cancer development. *Mol. Cancer Res.* 2006, *4*, 221–233.
- [3] Marx, J., Cancer immunology. Cancer's bulwark against immune attack: MDS cells. *Science* 2008, *319*, 154–156.
- [4] Gabrilovich, D. I., Nagaraj, S., Myeloid-derived suppressor cells as regulators of the immune system. *Nat. Rev. Immunol.* 2009, *9*, 162–174.
- [5] Gabrilovich, D. I., Ostrand-Rosenberg, S., Bronte, V., Coordinated regulation of myeloid cells by tumours. *Nat. Rev. Immunol.* 2012, *12*, 253–268.
- [6] Markiewski, M. M., DeAngelis, R. A., Benencia, F., Ricklin-Lichtsteiner, S. K. et al., Modulation of the antitumor immune response by complement. *Nat. Immunol.* 2008, *9*, 1225–1235.
- [7] Sinha, P., Okoro, C., Foell, D., Freeze, H. H. et al., Proinflammatory S100 proteins regulate the accumulation of myeloid-derived suppressor cells. *J. Immunol.* 2008, *181*, 4666–4675.
- [8] Bunt, S. K., Sinha, P., Clements, V. K., Leips, J., Ostrand-Rosenberg, S., Inflammation induces myeloid-derived suppressor cells that facilitate tumor progression. *J. Immunol.* 2006, *176*, 284–290.
- [9] Chornoguz, O., Grmai, L., Sinha, P., Artemenko, K. A. et al., Proteomic pathway analysis reveals inflammation increases

- myeloid-derived suppressor cell resistance to apoptosis. *Mol. Cell. Proteomics* 2011, 10, M110 002980.
- [10] Choksawangkarn, W., Kim, S. K., Cannon, J. R., Edwards, N. J. et al., Enrichment of plasma membrane proteins using nanoparticle pellicles: comparison between silica and higher density nanoparticles. *J. Proteome Res.* 2013, 12, 1134–1141.
- [11] Rahbar, A. M., Fenselau, C., Integration of Jacobson's pellicle method into proteomic strategies for plasma membrane proteins. *J. Proteome Res.* 2004, 3, 1267–1277.
- [12] Rahbar, A. M., Fenselau, C., Unbiased examination of changes in plasma membrane proteins in drug resistant cancer cells. *J. Proteome Res.* 2005, 4 (6), 2148–2153.
- [13] Chaney, L. K., Jacobson, B. S., Coating cells with colloidal silica for high yield isolation of plasma membrane sheets and identification of transmembrane proteins. *J. Biol. Chem.* 1983, 258, 10062–10072.
- [14] Kim, S. K., Choksawangkarn, W., Rose, R., Fenselau, C. et al., Nanowire pellicles for eukaryotic cells: nanowire coating and interaction with cells. *Nanomedicine (Lond)* 2013, 9(8):1171–1180.
- [15] Smolders, K., Lombaert, N., Valkenburg, D., Baggerman, G. et al., An effective plasma membrane proteomics approach for small tissue samples. *Scientific Reports* 2015, 5, 10917.
- [16] Sharma, P., Abbasi, C., Lazic, S., Teng, A. C. T. et al., Evolutionarily conserved intercalated disc protein Tmem65 regulates cardiac conduction and connexin 43 function. *Nature Communications* 2015, 6, 8391.
- [17] Aslakson, C. J., Miller, F. R., Selective events in the metastatic process defined by analysis of the sequential dissemination of subpopulations of a mouse mammary tumor. *Cancer Res.* 1992, 52, 1399–1405.
- [18] Pulaski, B. A., Ostrand-Rosenberg, S., Reduction of established spontaneous mammary carcinoma metastases following immunotherapy with major histocompatibility complex class II and B7.1 cell-based tumor vaccines. *Cancer Res.* 1998, 58, 1486–1493.
- [19] Ammar, S., Helfen, A., Jouini, N., Fievet, F. et al., Magnetic properties of ultrafine cobalt ferrite particles synthesized by hydrolysis in a polyol medium. *J. Mater. Chem.* 2001, 11, 186–192.
- [20] Bai, X., Son, S. J., Zhang, S., Liu, W. et al., Synthesis of superparamagnetic nanotubes as MRI contrast agents and for cell labeling. *Nanomedicine (Lond.)* 2008, 3, 163–174.
- [21] Wessel, D., Flugge, U. I., A method for the quantitative recovery of protein in dilute solution in the presence of detergents and lipids. *Anal. Biochem.* 1984, 138, 141–143.
- [22] Kessner, D., Chambers, M., Burke, R., Agus, D. et al., ProteoWizard: open source software for rapid proteomics tools development. *Bioinformatics*. 2008, 24, 2534–2536.
- [23] Edwards, N., Wu, X., Tseng, T.W., An unsupervised, model-free, machine-learning combiner for peptide identifications from tandem mass spectra. *Clinical Proteomics* 2009, 5, 23–36.
- [24] Edwards, N. J., PepArML, a meta-search peptide identification platform for tandem mass spectra. *Current Protocols Bioinformatics* 2013, 44, 23.1–23.
- [25] Ashburner, M., Ball, C. A., Blake, J. A., Botstein, D. et al., Gene ontology: tool for the unification of biology. The Gene Ontology Consortium. *Nat. Genet.* 2000, 25, 25–29.
- [26] Jang, J. H., Hanash, S., Profiling of the cell surface proteome. *Proteomics* 2003, 3, 1947–1954.
- [27] Huntley, R. P., Sawford, T., Mutowo-Muullenet, P., Shypitsyna, A. et al., The GOA database: Gene ontology annotation updates for 2015. *Nucleic Acids Res.* 2015, 43 (D1), D1057–D1063.
- [28] Zhang, B., VerBerkmoes, N. C., Langston, M. A., Uberbacher, E. et al., Detecting differential and correlated protein expression in label-free shotgun proteomics. *J. Proteome Res.* 2006, 5, 2909–2918.
- [29] Benjamini, Y. H. Y., Controlling the false discovery rate: a practical and powerful approach to multiple testing. *J. Roy. Stat. Soc. Ser. B (Methodological)* 1995, 57, 289–300.
- [30] Beissbarth, T., Hyde, L., Smyth, G. K., Job, C. et al., Statistical modeling of sequencing errors in SAGE libraries. *Bioinformatics*. 2004, 20 Suppl 1, i31–39.
- [31] Old, W. M., Meyer-Arendt, K., Aveline-Wolf, L., Pierce, K. G. et al., Comparison of label-free methods for quantifying human proteins by shotgun proteomics. *Mol. Cell. Proteomics* 2005, 4, 1487–1502.
- [32] Subramanian, A., Tamayo, P., Mootha, V. K., Mukherjee, S., B. L. et al., Gene set enrichment analysis: a knowledge-based approach for interpreting genome-wide expression profiles. *Proc. Natl. Acad. Sci.* 2005, 102, 15545–15550.
- [33] Cheng, P., Corzo, C. A., Luetetteke, N., Yu, B. et al., Inhibition of dendritic cell differentiation and accumulation of myeloid-derived suppressor cells in cancer is regulated by S100A9 protein. *J. Exp. Med.* 2008, 205, 2235–2249.
- [34] Burke, M., Choksawangkarn, W., Edwards, N., Ostrand-Rosenberg, S., Fenselau, C. Exosomes from myeloid derived suppressor cells carry biologically active proteins. *J. Proteome Res.* 2014, 13, 836–843.
- [35] Schmid, M. C., Varner, J., Myeloid cells in tumor inflammation. *Vascular Cell* 2012, 4, 1–7.
- [36] Haile, L. A., Gamrekelashvili, J., Manns, M. P., Korangy, F. et al., CD49d is a new marker for distinct myeloid-derived suppressor cell subpopulations in mice. *J. Immunol.* 2010, 185, 203–210.
- [37] Avraamides, C. J., Garmy-Susini, B., Varner, J. A., Integrins in angiogenesis and lymphangiogenesis. *Nat. Rev. Cancer* 2008, 8, 604–617.
- [38] Ridley, A. J., Schwartz, M. A., Burridge, K., Firtel, R. A. et al., Cell migration: integrating signals from front to back. *Science* 2003, 302, 1704–1709.